Journal of Power Sources 265 (2014) 282–290

Contents lists available at ScienceDirect

Journal of Power Sources

journal homepage: www.elsevier.com/locate/jpowsour

Analytical solutions for extended surface electrochemical fin models

Brice N. Cassenti, George J. Nelson, Matthew B. DeGostin, Aldo A. Peracchio, Wilson K. S. Chiu*

HeteroFoaM Center, A DOE Energy Frontier Research Center, Department of Mechanical Engineering, University of Connecticut, Storrs, CT 06269-3139, USA

HIGHLIGHTS

- Exact solutions were obtained to simulate current passages in SOFC electrodes.
- A solid oxide fuel cell (SOFC) electrode was selected as a test case for these studies.
- Assess geometry influence 3-D electrode microstructure on performance.
- Performance was correlated to geometrical changes in the electrode.

ARTICLE INFO

Article history:
Received 28 June 2013
Received in revised form
21 February 2014
Accepted 24 February 2014
Available online 2 May 2014

Keywords:
Analytical
Microstructure
SOFC
Conical
Spherical
Hyperbolic

ABSTRACT

Exact solutions were obtained for variations in the potential and the current for three axisymmetric geometries, with positive, negative and zero curvatures, which simulate current transport in fuel cell electrodes. These solutions can be used to assess the influence of geometry on performance for three dimensional electrode microstructures. A solid oxide fuel cell (SOFC) electrode was selected as a test case for these studies. From the exact solutions, simulations of current flow and potential drop for one dimensional networks in SOFC electrodes were performed. Numerical tests demonstrated that surfaces with positive curvature have greater current flow for the same potential drop due to higher current losses through the lateral surface area. The study also showed that zero curvature solutions will be sufficiently accurate for positive or negative curvature geometries for moderate radius changes, but differ significantly from positive or negative curvature solutions for more extreme radius changes. Analytical solutions indicate fundamental differences in geometry and its influence on current flow. Based on the results of the simulations, an approximate solution, based on one non-dimensional parameter, was developed for estimating the effects of extreme changes in cross-section area.

1. Introduction

The composite electrodes applied in electrochemical energy storage and conversion devices are heterogeneous functional material systems that must support the effective movement of charge generated by the electrochemical interaction between electrode phases. Such electrodes may include ceramic–metal (cermet) composites and mixed conducting electrodes found in solid oxide fuel cells (SOFCs) [1], carbon and transition metal oxide electrodes of Li-ion batteries [2,3], and porous titania films used in dye-sensitized solar cells [4,5]. These chemically active composite systems require the presence of sites that support fundamental chemistry and sufficient transport networks that deliver reactant species to and byproducts from these active sites. Considering these two key requirements, the deliberate design of microstructural geometry in composite electrodes can benefit performance by increasing the efficacy of active sites and by promoting the efficient movement of charge through conductive phases to the active surfaces.

Within SOFC electrodes, the effective transport of ions and electrons to active sites is of particular interest. In more common cermet electrodes, these sites reside where the solid ion and electron conducting phases meet an open pore phase that enables transport of gaseous reactants. In electrodes that support the mixed conduction of ionic and electronic charge carriers these reaction sites may be distributed over a broader portion of the solid–pore interface. It has generally been found that the extension of active

* Corresponding author.
E-mail address: wchiu@engr.uconn.edu (W.K.S. Chiu).

http://dx.doi.org/10.1016/j.jpowsour.2014.02.113
0378-7753/

Nomenclature

a	radius of cross-section, m
A_1, A_2	arbitrary constants
A_c	area of cross-section, m^2
A_{eff}	effective area of cross-section, m^2
A_s	surface area, m^2
i_c	total current through cross-section, A
I_1, K_1	modified Bessel functions of order one
k	curvature or slope, m^{-1}
L	segment length, m
ℓ	symmetric half segment, length, m
P_ν	Legendre function of order ν
R	charge transfer resistance, $\Omega\ m^2$
R'_c	equivalent cross-section resistance, Ω
R_s	equivalent surface resistance, Ω
r_o, r_e	entry and exit radii respectively, m
x	transformed axial coordinate $k(z - z_0)$
z	axial coordinate, m
z_0	axial offset, m
α	hyperbolic roots, $\pm\sqrt{1 + 2/\sigma Rk}$
β	equivalent circuit coefficient
Φ	transformed potential, φ/a
φ	potential, V

sites away from the planar interface between electrode and electrolyte layers of the cell can reduce overall polarization resistance within the electrode and increase SOFC performance. This extension is often achieved through the fabrication of a functional layer near the electrode/electrolyte interface with a finer microstructure than the porous electrode support. This extended active surface results in the more effective transfer of ionic charge carriers from the bulk electrolyte to active sites within the composite electrode [6,7].

The coupled electrochemistry and charge transport that occurs in these electrodes have been explored using a variety of techniques including thin-film electrode models [6,8], extended surface electrode models [7,9], and percolation theory [10–14]. A commonality in these modeling approaches is the application of a second order, ordinary differential equation comparable to the equation describing heat transfer from a thermal fin. Early application of this equation can be attributed to Kenjo et al. [6,8], who used a thin-film model to predict the polarization resistance of SOFC electrodes with varying composition and microstructural quality. This approach abstracted the dispersed ionic conducting phase as a thin film coating the electronic conducting phase and addressed both charge transport and microstructural geometry through the use of a single lumped parameter. It was found that materials that sintered well, forming wide contact areas between individual particles in the composite electrode, displayed superior performance compared to materials with poor sinterability. It was also demonstrated that for well sintered electrodes polarization resistance could be reduced by increasing the thickness of the active electrode. However, this improvement showed a diminishing return that suggests a trade-off between transport losses. The thin-film model of Kenjo et al. was adapted to an extended surface formalism by Tanner et al. [7], who treated the ionic conducting phase as a set of rectangular corrugations, coated with electrocatalyst, extending from the bulk electrolyte. This approach added microstructural detail by moving away from the lumped parameter description of charge transport and microstructure. Instead, microstructure was accounted for through the sizing and separation of the extended ion conducting surfaces. Other descriptions of charge transport within composite SOFC electrodes have drawn on percolation theory to define effective conductivity and other charge transfer parameters [10–14]. As in the analytical approaches provided by Kenjo et al. and Tanner et al., these approaches apply a governing equation comparable to that of a constant cross-section thermal fin.

The effects of varying particle contact geometry have been investigated by Zhao and Virkar [15] through the development of analytical expressions for the effective conductivity of sintered electrodes. The incorporation of more detailed microstructural geometry within extended surface electrode models was also explored by Nelson et al. [9] through the use of a governing equation that accounts for variable cross-section geometry in the extended surface. In this analysis, chains of ionic conducting particles extending from the electrolyte were simulated based on an iterated series of truncated cones. As illustrated in Fig. 1, these particle chains can be considered to comprise the active layer of the electrode that resides near the electrode–electrolyte interface. In electrodes with good connectivity such chains may extend into the porous electrode support. The variable cross-section extended surface approach was found to be capable of replicating experimentally observed polarization resistances in SOFC electrodes, inclusive of resistive effects linked to reduced interparticle contact areas that result when electrode particles are not sufficiently sintered [9]. Further investigation of the impacts of multi-dimensional transport and space charge regions at contact points between particles demonstrated that the analytical extended surface models provided an accurate assessment of electrode performance, particularly for purposes of screening potential microstructural designs [16]. Thus it has been found that variable cross-section extended surface models present a promising tool for the more deterministic design of electrode microstructures. However, the development of a more robust means of assessing electrode quality can benefit from extension of the electrochemical fin modeling concept to a more diverse set of particle shapes that may be present in electrode microstructures. For example, the fabrication of electrodes based on spherical particles has been demonstrated using samaria-doped ceria, and the conductivity of these porous composites has shown clear sensitivity to microstructural geometry [15].

In the present work exact analytical solutions are presented for a variety of particle shapes that may be used to simulate an extended surface electrode. These shapes include conical particles similar to those investigated previously [9,16], as well as particles with spherical shapes and particles with a profile based on a hyperbolic cosine function. These latter two particle profiles are illustrated in Fig. 1b. Using a set of basic parametric studies, transport effects associated with particle curvature, variable cross-sectional area, surface area, and length are investigated to further elucidate the role of microstructural geometry in electrode performance. The effects of material properties and boundary conditions are included in the solutions and can also be addressed to better determine the interaction between particle shape and the physical phenomena that govern electrode operation. For example, the effects of curvature on surface current losses can be examined since exact solutions for positive (spherical surface), zero (conical surface) and negative (hyperbolic surface) curvatures have been developed. Hence, even small differences in current loss can be used to find trends. The analytical solutions have shown conclusively that positive

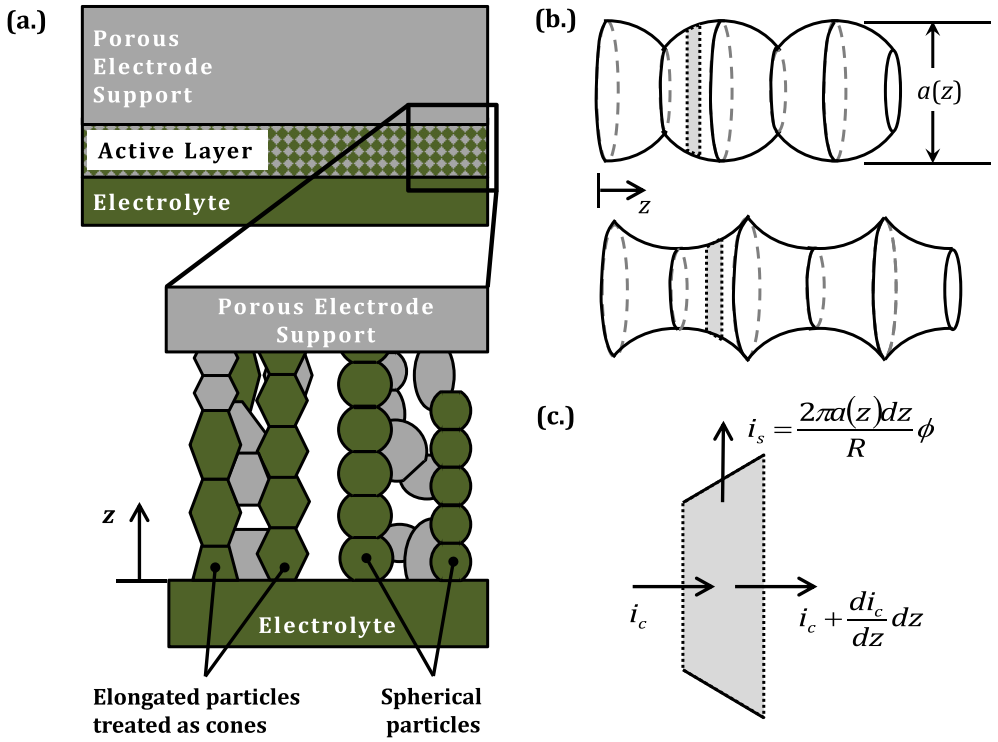

Fig. 1. To formulate an extended surface electrode model, the active layer of a composite electrode (a.) is treated as a network of particle chains supporting the conduction of ions away from the bulk electrolyte. The particles comprising such chains may be approximated using several shapes including: conical (a.), spherical (a. and b.), and hyperbolic (b.). The governing equation for charge transport in these variable cross-section structures may be developed by taking a charge balance on a differential control volume (c.) within the structure.

curvatures will have a greater loss than negative, with zero curvature producing an intermediate result.

2. Model formulation

The governing equations, that establish the analytical model presented here, are developed based on an extended surface of charge conducting material subject to a charge transfer reaction at its surface. As illustrated in Fig. 1, the profile of this extended surface may take a number of shapes. However, to permit the cross-sectional averaging of the potential within the structure, these shapes must be axisymmetric. Two key assumptions are applied with respect to transport in the solid cross-section of the extended surfaces considered. First, one dimensional transport is assumed along the length of these extended surfaces in the *z*-direction. In previous investigations this approximation has been found to hold for most cross-sectional geometries [16]. An exception to the sufficiency of this assumption is found for particles with contact radii that are significantly smaller than the largest particle radius, i.e. a high gradient in particle cross-sectional area. In such cases, the one-dimensional approximation overestimates performance predictions. Second, in the analytical model presented the flow of charge within the solid phase is treated as ohmic, with space charge effects neglected. In contact regions between individual particles, grain boundaries may lead to the formation space charge regions, which display a higher resistance to transport than the material in the bulk particle [15,17]. As in the case of multidimensional transport, neglecting the additional resistance introduced by these space charge regions leads to an overestimate of electrode performance by the analytical models [16]. In general, the analytical approach presented in this work proves sufficient as a meso-scale screening tool for assessing the quality of SOFC electrode microstructures that may be produced using emerging fabrication techniques.

Considering the case of one-dimensional transport in the absence of space charge effects, the flow of current within the solid cross-section may be defined according to Ohm's law.

$$i_c = -\sigma A_c(z)\frac{d\varphi}{dz} \tag{1}$$

Here, σ is the conductivity of the solid phase, A_c is the cross-sectional area, and φ is a potential difference between the solid phase and a reference potential. Details of the definition of this reference potential are provided by Nelson et al. [9].

To permit development of an analytical model a linear description of the surface charge transfer reaction is applied. For an SOFC electrode this approximation is considered to hold when gas transport is fast within the pores of the electrode. In such a case, the relative rate of charge transfer may be approximated using a charge transfer resistance. Based on this approximation a current related to the surface charge transfer may be defined in terms of the potential difference, φ, the surface area, A_s, and the charge transfer resistance, R.

$$i_s = \int_{A_s} \frac{\varphi\, dA_s}{R} \tag{2}$$

With the solid phase current, i_c, and surface charge transfer current, i_s, defined the governing equation for the analytical model may be developed. This is done by defining a differential control volume within the extended surface structure and subsequently taking a charge balance on this volume, as illustrated in Fig. 1c. For

this development the cross-sectional and surface areas are defined for a generic axisymmetric structure according to the local radius, $a(z)$, as shown in Eqs. (3) and (4). The charge balance, in terms of the currents is given according to Eq. (5).

$$A_c(z) = \pi a^2(z) \tag{3}$$

$$dA_s(z) = 2\pi a(z)\sqrt{1+\left(\frac{da}{dz}\right)^2}dz \tag{4}$$

$$\left(i_c + \frac{di_c}{dz}dz\right) - i_c - \frac{2\pi a(z)\sqrt{1+\left(\frac{da}{dz}\right)^2}dz}{R}\varphi = 0 \tag{5}$$

Substituting Eq. (1) for the solid phase current and rearranging terms results in an ordinary differential equation describing the potential difference within the structure.

$$a^2(z)\frac{d^2\varphi}{dz^2} + 2a(z)\frac{da}{dz}\frac{d\varphi}{dz} - \frac{2a(z)}{\sigma R}\sqrt{1+\left(\frac{da}{dz}\right)^2}\varphi = 0 \tag{6}$$

In Eq. (6) the conductivity, σ, and the charge transfer resistance, R, are constant functions of z. Eq. (6) governs the variation in the potential for axisymmetric geometries for a radius that is an arbitrary function of axial position. Note that there is a multiple of the radius in each of the three terms that can be removed. Boundary conditions, for Eq. (6), include a specified potential, φ, a specified current, i_c, or a linear combination of the potential and current.

3. Exact solutions

Exact solutions remove the uncertainty from numerical approximations, allowing interpretations to be confidently made from small differences in the results. To determine the influence of various parameters geometries have been chosen for which exact solutions can be found. However, the square root in Eq. (6) makes it difficult to find exact solutions for the potential. Exact solutions for three geometries, including spherical segments, conical segments and a hyperbolic geometry, have been developed as an aid in determining the influence of curvature. Three parameters will be used to describe the geometry: 1) the length of the segment, L, 2) a curvature, or slope, parameter, k, and 3) an offset, z_0.

3.1. Conical solution

Conical segments have a linear variation in the radius, making the square root a constant in Eq. (6) and, thus, eliminating the complication from the square root. We use for the radius

$$a = kz + z_0. \tag{7}$$

Transforming the independent variable from z to a Eq. (6) becomes

$$a\frac{d^2\varphi}{da^2} + 2\frac{d\varphi}{da} - \frac{2\sqrt{1+k^2}}{\sigma R k^2}\varphi = 0 \tag{8}$$

Eq. (8) can be converted to a standard Bessel function differential equation by setting

$$x = 2\sqrt{\frac{2(1+k^{2)})}{\sigma R k}}a. \tag{9}$$

Eq. (8) becomes

$$x^2\frac{d^2\varphi}{dx^2} + x\frac{d\varphi}{dx} - x^2\varphi = 0. \tag{10}$$

The general solution of Eq. (10) is

$$\begin{aligned}\varphi &= A_1 I_1(x) + A_2 K_1(x)\\ &= A_1 I_1\left(2\sqrt{\frac{2(1+k^{2)})}{\sigma R k}}(kz+z_0)\right)\\ &\quad + A_2 K_1\left(2\sqrt{\frac{2(1+k^{2)})}{\sigma R k}}(kz+z_0)\right)\end{aligned} \tag{11}$$

where A_1 and A_2 are arbitrary constants, evaluated by the boundary conditions at $x = 0$, and $x = L$, and I_1, K_1 are modified Bessel functions of order one of the first and second kind, respectively.

3.2. Spherical solution

For the case of a spherical segment the radius is

$$a^2 + (z - z_0)^2 = \frac{1}{k^2}. \tag{12}$$

Substituting Eq. (12) into Eq. (6) the governing equation for the potential becomes

$$\left(\frac{1}{k^2} - (z-z_0)^2\right)\frac{d^2\varphi}{dz^2} - 2z\frac{d\varphi}{dz} - \frac{2}{\sigma R k}\varphi = 0. \tag{13}$$

Eq. (13) can be simplified by the substitution

$$x = k(z - z_0), \tag{14}$$

which yields the form

$$\left(1 - x^2\right)\frac{d^2\varphi}{dx^2} - 2x\frac{d\varphi}{dx} - \frac{2}{\sigma R k}\varphi = 0. \tag{15}$$

Eq. (15) is the Legendre equation and has the solution

$$\begin{aligned}\varphi &= A_1 P_{\nu(1)}(x) + A_2 P_{\nu(2)}(x)\\ &= A_1 P_{\nu(1)}(k(z-z_0)) + A_2 P_{\nu(2)}(k(z-z_0))\end{aligned} \tag{16}$$

where A_1 and A_2 are arbitrary constants and $\nu(1,2) = -1/2 \pm \sqrt{(1/2)^2 + (2/\sigma R k)}$. A series solution about $x = 0$ was developed for this equation. One series begins at x^0 and contains only even powers of x. The second begins at x^1 and contains only odd powers of x. The radius of convergence of the series is one and hence does not extend past the singular points $x = \pm 1$. That is, the series does not converge at or beyond the poles of the sphere. This convergence behavior is considered sufficient because a particle that is a complete (i.e. non-truncated) sphere would represent an unsintered geometry, and therefore be a non-functional electrode microstructure.

3.3. Hyperbolic solution

A solution for a hyperbolic geometry can be attained by noting that if $da/dz = \sinh(k(z-a))$ (i.e., take $a(z) = 1/k\cosh(k(z-z_0))$) then $\sqrt{1+(da/dz)^2} = \cosh(k(z-z_0))$. For φ proportional to $\sinh(k(z-z_0))$ each term in Eq. (6) will contain the factor $\cosh^2(k(z-z_0))\sinh(k(z-z_0))$.

Using

$$a(z) = \frac{1}{k}\cosh(k(z - z_0)) \tag{18}$$

and substituting Eq. (18) into Eq. (6) the governing equation for the potential is

$$\left(1 + x^2\right)\frac{d^2\varphi}{dx^2} + 3x\frac{d\varphi}{dx} - \frac{2}{\sigma R k}\varphi = 0 \tag{19}$$

where $x = \sinh(k(z - z_0))$. Note the similarity between Eq. (19) and Eq. (15). The change in sign of x^2 in the first term illustrates the change in curvature of the surface. As in the case of the spherical segment, a series solution about $x = 0$ can be developed. One series will begin at x^0 and contain only even powers of x. The second will begin at x^1 and contain only odd powers of x. Unfortunately, the radius of convergence of the series is one and hence does not extend past $x = \pm 1$. The poles in this case are at $x = \pm i$, but the series diverges when $|x| = |\sinh(k(z - z_0))| \geq 1$. Hence a more general solution needs to be developed to move beyond $x = \pm 1$.

A new solution can be developed by changing the dependent variable in Eq. (6). In a manner analogous to the solution of the transient diffusion equation in spherical coordinates, let

$$\varphi = \frac{\Phi}{a(z)}. \tag{20}$$

Eq. (6) becomes

$$\frac{d^2\Phi}{dz^2} - \frac{1}{a}\left[\frac{d^2a}{dz^2} + \frac{2}{\sigma R}\sqrt{1 + \left(\frac{da}{dz}\right)^2}\right]\Phi = 0. \tag{21}$$

Substituting for the radius from Eq. (18) results in

$$\frac{d^2\Phi}{dz^2} - k^2\left[1 + \frac{2}{\sigma R k}\right]\Phi = 0. \tag{22}$$

This equation can be readily solved to yield

$$\Phi = A_1 e^{\alpha x} + A_2 e^{-\alpha x}, \tag{23}$$

where $\alpha = \sqrt{1 + 2/\sigma R k}$, $x = k(z - z_0)$, and A_1, A_2 are arbitrary constants.

3.4. Composite solution

The individual general solutions, Eqs. (11), (16) and (23), can readily be combined to build a composite structure. Each segment of the structure is described by the nodes at each end, the geometric parameters (*particle length, particle curvature and offset*), the conductivity, and the charge transfer resistance. The potential at the nodes are the unknowns, and the governing equations are generated by requiring continuity of the current (i.e., the sum of the currents entering a node minus the sum of the currents leaving a node is zero.)

4. Parametric simulations

Computer codes have been written based on these solutions to simulate arbitrary structures using the exact solutions for a conical, spherical and hyperbolic geometry. Two versions of the code have been developed: 1) a MATLAB version and 2) an Excel version offset with Visual Basic. Each version has its own advantages and disadvantages. The Excel version is easily ported from machine to machine. The MATLAB version can readily accommodate a model with many segments.

Nine cases with realistic parameters were considered as shown in Fig. 2. There are three cases for each of the signs in the curvature. In each case the radius varies by a factor of two from the minimum to the maximum. The first case consists of one segment with the larger radius at twice the potential of the smaller radius. The curvature geometry also has two, two segment versions: one with the minimum radius at the center and one with the maximum radius at the center.

Fig. 2 shows that the input current is approximately the same for each of the two segment cases, but there is a significant difference for the single segment cases. This result appears to be due to the fact that the average area of the cross-section for the spherical case is larger while the hyperbolic case has a smaller average area. The conical segment is intermediate. The current loss out the surface though is largest for the spherical segment, smallest for the hyperbolic segment, and again is intermediate for the conical segments. The two segment cases, when compared for each geometry, show it makes little difference where the minimum radius is located.

Fig. 3 shows an investigation of potential as a function of axial location in the three geometries: spherical, conical, and hyperbolic. It appears that the conical segment provides a good approximation over moderate changes in radius, and should provide accurate current predictions for the spherical and hyperbolic cases if enough conical segments are used across a single spherical or hyperbolic segment to capture the non-zero curvature.

To evaluate how neck size affects the influence of geometry on the current flow, a radius ratio parameter is defined as the ratio of the end radius of a particle to the neck radius that serves as the contact area between two artificially sintered particles. Varying this radius ratio about that which is shown in Fig. 2 for each of the two-segment cases allows the model to assess the influence that constrictive effects have on current flow for these different geometries.

Fig. 4 is a plot of resistance per unit length that results from setting a constant current flux boundary condition at one end of the two-segment particles and fixing a zero potential at the opposite end. This value is plotted for varying radius ratios for when the minimum radius and maximum radius are at the center, respectively. In this figure it appears that increased deviation from the cylindrical case of $r_{end}/r_{neck} = 1$ yields a higher equilibrium potential, regardless of the curvature geometry. This is due to constrictive effects of the reduced neck size between sintered particles when the minimum radius is at the center, and reduced cross sectional area for current to flow at the ends of the sintered particles when the maximum radius is at the center.

The results in Fig. 4 also indicate that as the radius ratio deviates further from the value of two, presented in Fig. 2, the aforementioned differences between curvature geometries are more pronounced. This becomes most apparent for extreme ratios of 0.1 and 10, where greater differences in cross sectional area variation for each geometry type more significantly affect the resulting current flow. In these cases, hyperbolic particles exhibit the highest resistance per unit length, while spherical particles are lowest. Conical particles showcase intermediate results. This implies that along the primary transport direction, spherical particles provide the least resistance to the flow of ions due to a greater cross sectional area along their length than corresponding conical and hyperbolic particles.

5. Approximate solution

The results presented can be used to provide insight into how microstructure affects the performance. Also, it would be very

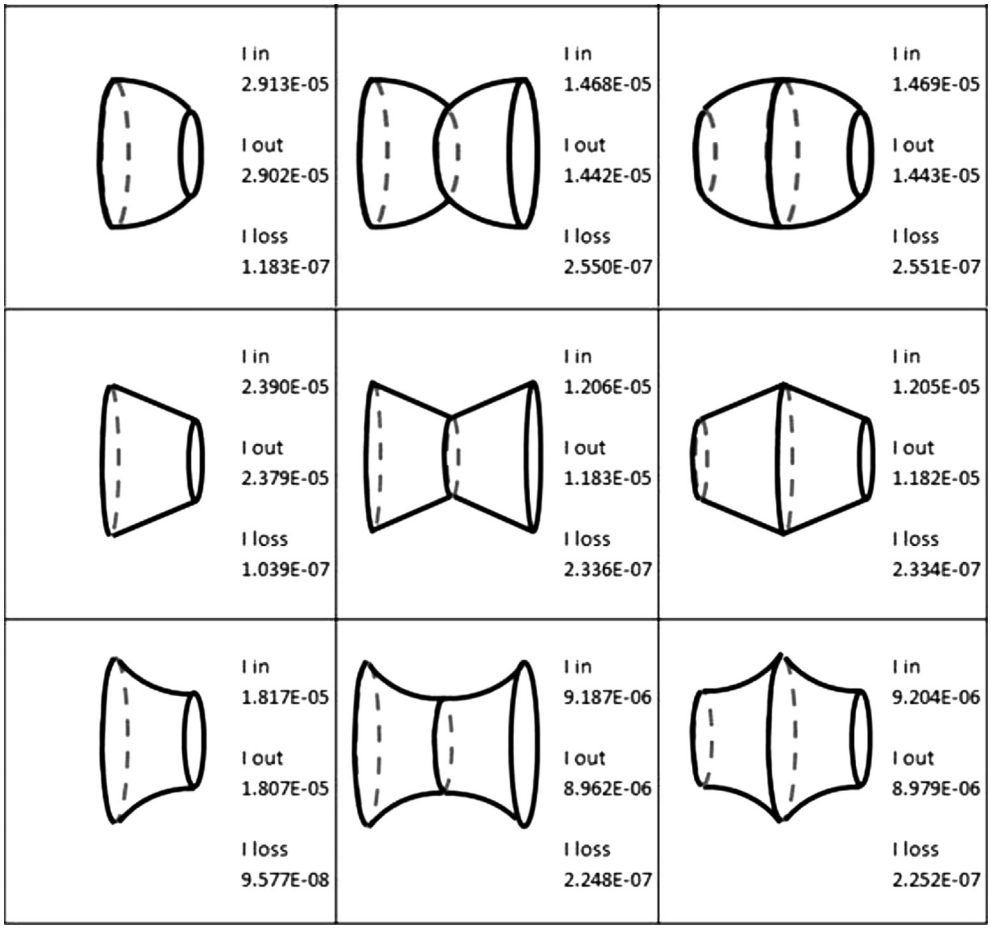

Fig. 2. Current loss through the surface of various composite structures illustrates that a positive curvature (spherical segment) will have a greater loss than a zero (conical segment) or negative (hyperbolic segment) curvature. In all nine cases the larger radius is twice the smaller. All segments have the same length. The current enters from the left surface (I_{in}), and exits to the right surface (I_{out}). Current is lost through the side surfaces as indicated by I_{loss}. All current values have units of A m^{-2}. One or two particles were connected as shown. The area ratio (maximum to minimum) was four in all cases. The conductivity (10 S m^{-1}) and surface loss coefficient (10^{-4} Ω) was the same for all examples.

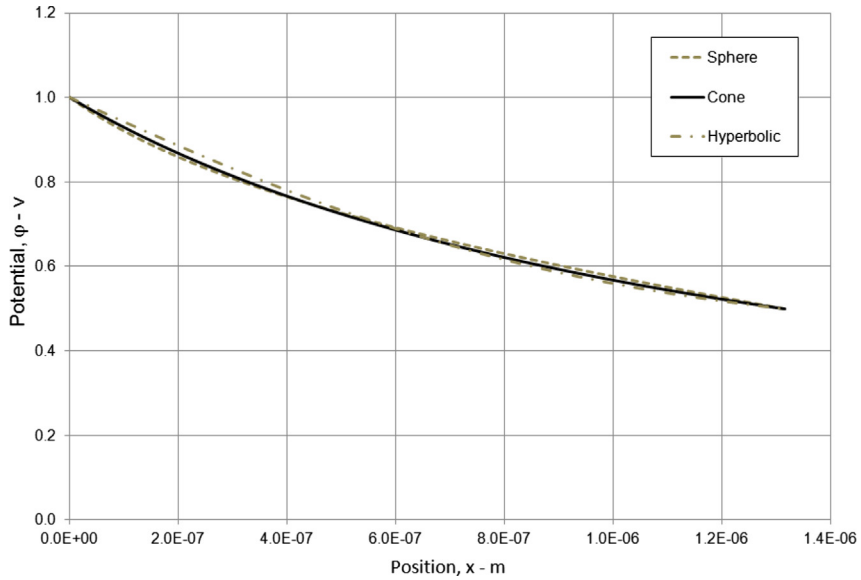

Fig. 3. The effect of curvature on potential in a single segment illustrates that more rapid changes in potential indicate more current loss through the surface. The radius at current entry ($x = 0$) is twice as large as the radius of at current exit.

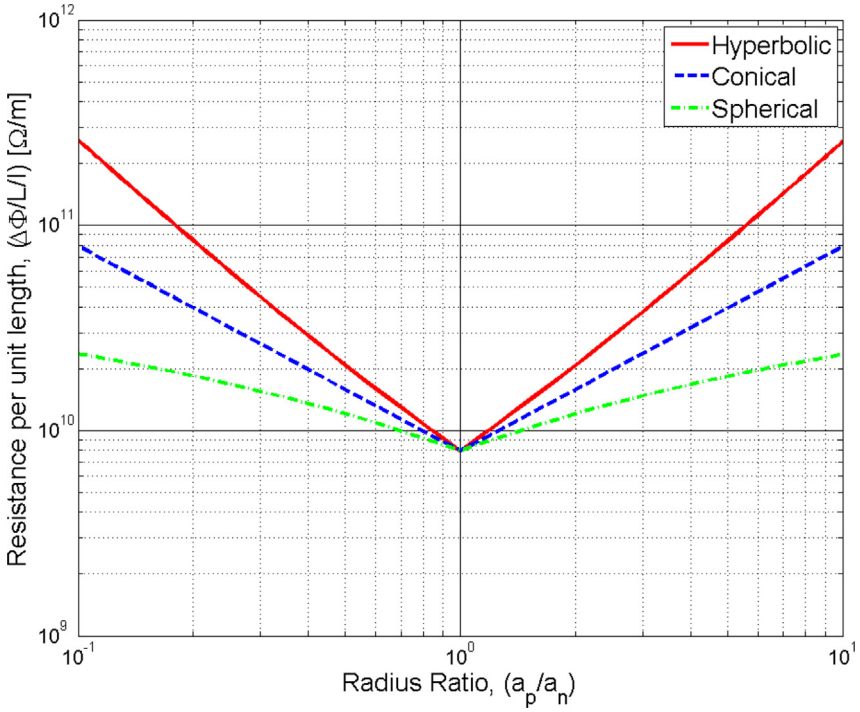

Fig. 4. Resistance per unit length shown as a function of radius ratio for sintered particles of each geometry illustrates that as the radius ratio deviates from the case of a cylinder ($r_{end}/r_{neck} = 1$), current flow is increasingly impacted by the curvature geometry.

useful for design estimates to develop an accurate approximate analysis. We can develop an estimate by considering the current flowing in the circuit in Fig. 5. In the figure current leaving the surface is assumed to go to the ground potential through the resistor at the center of the segment. The conduction path with currents in, I_{In}, and out, I_{Out}, has a total resistance of $R'_c = L/(\sigma A_{eff})$ where σ is the conductivity, L is the total segment length, and A_{eff} is the effective conduction cr-sectional area. The resistor to ground has a total resistance of R_s/A_s, where A_s is the total surface area but is weighted by the potential. If the current, over an average, is assumed to see half the potential then the effective surface resistance is $R'_s = 2R_s/A_s$. The circuit can now be readily solved to yield

$$\frac{I_s}{I_{In}} = \frac{1/2[L/(\sigma R_s)]\left(A_s/A_{eff}\right)}{1 + 1/2[L/(\sigma R_s)]\left(A_s/A_{eff}\right)} \tag{24}$$

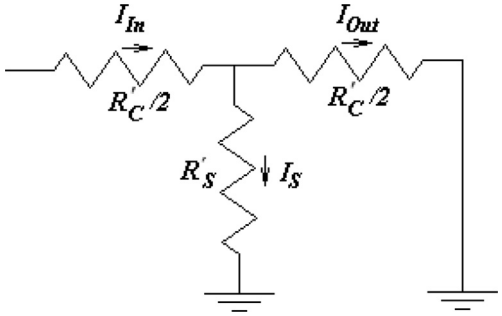

Fig. 5. Equivalent resistor circuit for a single segment consists of three resistors. The surface losses are represented by the resistor R_S and the axial resistance, R_C, is divided into two equal parts before and after resistor R_S. The currents in and out of the segment are I_{In} and I_{Out} respectively, and the current lost through the surface is I_S.

where I_S is the current lost through the surface. In Eq. (24) we have taken the surface area to be the actual surface area of the segment, that is

$$A_s = \int_0^L 2\pi r\sqrt{1 + \left(\frac{dr}{dx}\right)^2}\,dx. \tag{25}$$

For the equivalent cross-sectional area consider the current, I, through a cross-section where

$$I = \sigma A_c(x)\frac{d\phi}{dx} \tag{26}$$

and $A_c(x)$ is the cross-section area at location x at potential ϕ.

The total change in the potential across the length L, for no loss through the surface ($R_s = \infty$), is

$$\Delta\phi = \frac{I}{\sigma}\int_0^L \frac{dx}{A_c(x)} = \frac{IL}{\sigma A_{eff}} \tag{27}$$

which can be used to define the equivalent cross-section area, A_{eff}, as:

$$\frac{1}{A_{eff}} = \frac{1}{L}\int_0^L \frac{dx}{A_c(x)}. \tag{28}$$

For the three geometries for which we have exact solutions the effective cross-section area and the total surface areas can be found analytically. For the conical geometry symmetric about the origin, $x = 0$, the radius varies according to:

$$r(x) = r_e + \left(\frac{r_o - r_e}{\ell}\right)x, \tag{29a}$$

the effective cross-section over $-\ell \le x \le \ell$ is given by:

$$A_{eff} = \pi r_o r_e, \tag{29b}$$

and the surface area is

$$A_s = 2\pi\sqrt{1 + \left(\frac{r_o - r_e}{\ell}\right)^2}(r_o + r_e)\ell. \tag{29c}$$

For the spherical geometry symmetric about the origin the radius varies according

$$r(x) = \sqrt{R^2 - x^2}, \tag{30a}$$

the effective cross-section over $-\ell \le x \le \ell$ is given by:

$$A_{eff} = \frac{2\pi R\ell}{\ln\left(\frac{R+\ell}{R-\ell}\right)} \tag{30b}$$

and the surface area is

$$A_s = 4\pi R\ell. \tag{30c}$$

Last for the hyperbolic geometry symmetric about the origin the radius varies according to:

$$r(x) = \frac{1}{k}\cosh(kx), \tag{31a}$$

and the effective cross-section over $-\ell \le x \le \ell$ is given by:

$$A_{eff} = \frac{\pi\ell}{k\tanh(k\ell)}, \tag{31b}$$

and the surface area is

$$A_s = \frac{2\pi}{k^2}\left[k\ell + \frac{1}{2}\sinh(2k\ell)\right]. \tag{31c}$$

Note that for all three cases the total length $L = 2\ell$ Eqs. (29)–(31) can be used to arrive at values for combinations of geometries by applying the definition for the effective cross-section area.

Eq. (24) can now be generalized by using a parameter, β, to absorb some of the inaccuracies due to the assumption that the surface resistance is connected at the center of a symmetric segment. The approximation can be written as:

$$\frac{I_S}{I_{In}} = \frac{\beta/2[L/(\sigma R_S)]\left(A_S/A_{eff}\right)}{1 + \beta/2[L/(\sigma R_S)]\left(A_S/A_{eff}\right)}. \tag{32}$$

A least square error fit was used to find β from simulations on the symmetric geometries presented. The best fit was given by a value of 1.098 for β. The best fit for the symmetric geometries considered is shown in Fig. 6. The results in Fig. 6 appear accurate and are qualitatively the same as those presented in Fig. 4 of reference [18]. Hence the approximation in Eq. (32) can be used to accurately predict the fin effectiveness. A single parameter, $[L/(\sigma R_S)](A_S/A_{eff})$, appears to be sufficient to represent the response of symmetric geometries. The parameter is the product of the axial resistance relative to the surface resistance and the surface area relative to the axial area. Values for the parameter only need to be accurate to within a factor of 1.7. A value of 1.098 for β represents a resistance of $0.551R'_c$ in Fig. 5. Note that if β is exactly one then the approximation in Eq. (24) would result, and the axial resistance would connect to the surface resistor at its center as in Fig. 5.

6. Conclusions

Exact solutions have been obtained for the variation in the potential and current for three axisymmetric geometries: a spherical geometry (positive curvature), a conical geometry (zero curvature)

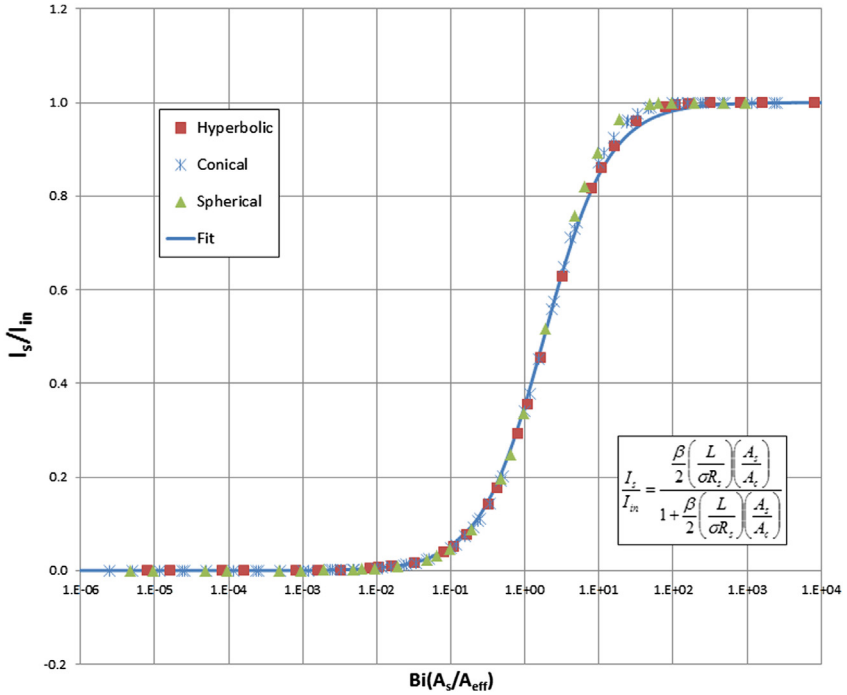

Fig. 6. A comparison of the approximate solution using $\beta = 1.098$ with the results for various symmetric geometries accurately predicts the fin effectiveness for the symmetric geometries investigated. Note that most of the performance change occurs over a single decade in the nondimensional parameter $0.25 \le \mathrm{Bi}(A_S/A_C) \le 2.5$ which agrees with the results presented in Ref. [18].

and a hyperbolic geometry (negative curvature). The solutions can be used to accurately assess the influence of geometry. Geometries with positive curvature have more current flow for the same potential drop and the same change in radius, but lose more current through the lateral surface area. Conical segments will be sufficiently accurate for moderate changes in radius if several segments are used to represent a single spherical or hyperbolic segment. The mathematics in the derivation of the solutions illustrate the fundamental difference in the geometries and the influence of geometry on potential variations and current flow.

An approximate solution was developed that provides a quick and accurate assessment of changes in geometry and material properties. A single dimensionless parameter combining physical parameters and geometric parameters appears to be sufficient for representing the performance of symmetric particles. This can provide insight into the effects of microstructure on performance and can aid in the design of new microstructures without the need for detailed analysis.

Acknowledgments

Financial support from an Energy Frontier Research Center on Science Based Nano-Structure Design and Synthesis of Heterogeneous Functional Materials for Energy Systems (HeteroFoaM Center) funded by the U.S. Department of Energy, Office of Science, Office of Basic Energy Sciences (Award DE-SC0001061) is gratefully acknowledged.

References

[1] W.K.S. Chiu, A.V. Virkar, F. Zhao, K.L. Reifsnider, G.J. Nelson, F. Rabbi, Q. Liu, J. Fuel Cell Sci. Technol. 9 (2012).
[2] M. Park, X. Zhang, M. Chung, G.B. Less, A.M. Sastry, J. Power Sources 195 (2010) 7904–7929.
[3] J.W. Fergus, J. Power Sources 195 (2010) 939–954.
[4] M. Grätzel, Acc. Chem. Res. 42 (2009) 1788–1798.
[5] J. Bisquert, Phys. Chem. Chem. Phys. 10 (2008) 49–72.
[6] T. Kenjo, S. Osawa, K. Fujikawa, J. Electrochem. Soc. 138 (1991) 349–355.
[7] C.W. Tanner, K. Fung, A.V. Virkar, J. Electrochem. Soc. 144 (1997) 21–30.
[8] T. Kenjo, M. Nishiya, Solid State Ionics 57 (1992) 295–302.
[9] G.J. Nelson, A.A. Peracchio, W.K.S. Chiu, J. Power Sources 196 (2011) 4695–4704.
[10] S. Sunde, J. Electroceram. 5 (2000) 153–182.
[11] P. Costamagna, P. Costa, V. Antonucci, Electrochim. Acta 43 (1998) 375–394.
[12] M. Cannarozzo, S. Grosso, G. Agnew, A. Del Borghi, P. Costamagna, J. Fuel Cell Sci. Technol. 4 (2007) 99–106.
[13] S. Sunde, J. Electrochem. Soc. 143 (1996) 1123–1133.
[14] S. Sunde, J. Electrochem. Soc. 143 (1996) 1930–1939.
[15] F. Zhao, A.V. Virkar, J. Power Sources 195 (2010) 6268–6279.
[16] G.J. Nelson, B.N. Cassenti, A.A. Peracchio, W.K.S. Chiu, J. Power Sources 205 (2012) 48–56.
[17] X. Guo, J. Maier, J. Electrochem.Soc. 148 (2001) E121–E126.
[18] J. Fleig, J. Maier, J. Eur. Ceram. Soc. 24 (2004) 1343–1347.